2015 IEEE International Conference on Robotics and Automation (ICRA)
Washington State Convention Center
Seattle, Washington, May 26-30, 2015

Depth Image Based Gait Tracking and Analysis via Robotic Walker

Chung Dial Lim, Ching-Ying Cheng, Chia-Ming Wang, Yen Chao, and Li-Chen Fu, *Fellow, IEEE*

***Abstract*— In this paper, we propose a gait tracking and analysis method using a depth image sensor installed on robotic walker. Nowadays, robotic walker not only can assist elders who have suffered deteriorating mobility but also help to provide rehabilitating function to people who have crippled walking ability. This approach is meant to be sufficiently accurate, non-intrusive, and low-cost. The goal of this research is to enable the robotic walker to become more active in terms of walker control and comfortable user experiences thorough gait analysis. In experiment, the accuracy of the proposed 3D leg pose tracking method was evaluated by a motion capture system and the result is quite promising. After actual trials, the proposed method has the potential to be used in a safer and more reliable application such as those assisting elders and specific group of patient subjects.**

I. INTRODUCTION

For human, mobility is the major condition to maintain their body function. However, most elders would have some handicaps for ambulation because of chronic disease or decline of muscular strength. Therefore, the issues have emerged with the coming of aging societies due to the improvement of medication and fertility decline, such as a shortage of caregivers and higher proportion of elders who need to assistance in daily life. Thus, the dependency ratio is becoming imbalanced nowadays.

In recent years, assistive technology product is expected to solve the insufficient of the nursing resources, especially for the elderly caring. Many of aiding devices have been developed for assistance or therapeutic purpose. A current research topic is the use of robotic walkers for elders. Various robotic walkers have been developed nowadays. Motorized active walkers with gait analysis capability is believed to provide safer platform for elders to stabilize their gait.

In general, human gait assessment has been widely studied in many different research experiments using two major pieces of equipment. These important pieces are known as the wearable sensors and the camera based systems. Although the wearable devices provide the accurate motion data for the gait assessment, it might not guarantee a comfortable experience for the users who are wearing devices. On the other hand, in order to deal with the high cost of motion capture systems which are restricted to just a laboratory environment, there are some human gait analysis approaches with a single view camera that have been developed. [1] proposed a low cost marker-less human motion capture system for gait analysis. A set of 3D position key points of the human body defined by the author and the tracking of motion was used by their proposed Interval Particle Filtering method. [2] presents a view-invariant marker-less model based approach with a single camera for gait analysis. Instead of focusing on sagittal view motion capture, [3] proposes a frontal view gait recognition by extracting the unique signatures from the descriptors of a silhouette's deformation. The assessment for the gait disorder which is measured by the depth camera is also investigated in [4]. However, these research models are assumed from the images with located salient parts such as the torso or head. It is not suited to our problem that only the lower limb is observed in the image. [5] proposed vision-based tracking system that estimates the 3D pose of lower limb of a wheeled walker (conventional walker) user's with a Kinect, where the author adopted the particle filtering method to estimate the 3D leg pose and obtained the spatio-temporal gait parameters. However, the dimension of the estimated states are too large and thus it is unable to the realized in real time to provide the corresponding assistance to user.

The goal of this research is to provide a real time 3D leg pose tracking and gait analysis method which is completely non-intrusive by using depth camera.

II. SYSTEM OVERVIEW

Figure 1. The system architecture of gait tracking and analysis on robotic walker.

Fig. 1 shows the system architecture of gait tracking and analysis on robotic walker. The human gait analysis from frontal view is proposed, where the depth image is captured by depth camera mounted on the rear (user side) of robotic walker for gait analysis (shown in Fig. 2).

Due to the fact that only shank and foot are observed in the depth image, leg segmentation is conducted before the leg pose is being tracked, which facilitates us to eliminate some redundant information such as the background and floor. In the beginning of the 3D leg pose tracking, the ankle joint is identified by calculating the curvature on leg surface, which is the important feature from frontal view to separate the shank and foot. For leg tracking, the sampling process of

[1]Chung Dial Lim is with the Department of Computer Science, National Taiwan University, Taiwan. (e-mail:r01922153@csie.ntu.edu.tw).

[2]Ching-Ying Cheng is with the Department of Computer Science, National Taiwan University, Taiwan. (e-mail:r02944023@csie.ntu.edu.tw).

[3]Chia-Ming Wang is with the Department of Electrical Engineering, National Taiwan University, Taiwan. (e-mail:d01921028@ntu.edu.tw).

[4]Yen Chao is with the Department of Computer Science, National Taiwan University, Taiwan. (e-mail:r03944011@ntu.edu.tw).

[5]Li-Chen Fu is with the Department of Electrical Engineering and Computer Science and Information Engineering, NTU, Taipei, Taiwan (phone: 886-2-23622209;e-mail: lichen@csie.ntu.edu.tw)

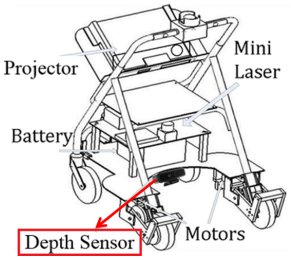

Figure 2. Robotic platform with depth camera mounted on the rear (user side) of robotic walker.

particle are modeled as a cylinder for fitting the lower limb. Then, we can extract the 3D points of ankle, tiptoe and top shank of each leg for monitoring the position of human foot. In gait analysis, the gait cycle and spatio-temporal gait parameters such as step length and step velocity can be derived for the user gait assessment.

III. Walking Gait Tracking and Analysis

The raw 3D point cloud from depth sensor contains redundant information in the dynamic and uncertain environment. For instance, the background and floor may cause failure to detect the user's lower limbs. Therefore, we apply two filters to extract the foreground. First, the 3D points are filtered as the background if depth value z is greater than 120cm, due to the fact that most of the users move within the region which is within 120cm far from the walker. Second, we adopt the Random Sample Consensus (RANSAC) [6] algorithm to subtract the floor plane. Note that we assume the floor is flat and clear, thus floor capturing is proposed only when the system initializes. Finally, the foreground 3D data are considered in association to the user's lower limbs.

A. Ankle Joint Identification

To identify both parts of the leg (shank and foot), the most significant feature is the ankle joint, because the ankle joint connects the shank and the foot. This surface performs an intense curve on the area between the area in which the shank and foot meet. This is a strong feature which allows us to identify the position of the ankle joint in depth image. Therefore, the goal is to estimate ankle joint by calculating curvature value of the leg.

First, we apply Canny edge detectors for the contour of the leg. We then construct a skeleton for each leg. Fig. 3(a) shows the leg's skeletal points constructed along the y-axis in the image. Skeletal point p^s of a leg is the center position between the left contour position p_{c_l} and the right contour position p_{c_r} as shown by equation (1). The function $k(p^s)$ is an organized skeleton (referring in equation (2)) along N skeletal points, which produces depth value z where p^s locates in depth image. Each skeletal point of left skeleton, denoted as p^s_{left}, and right skeleton, denoted as p^s_{right}. Fig. 3(b) shows depth values of the skeleton of left leg.

$$(x,y)_{p^S} = \frac{(x,y)_{p_{c_l}} + (x,y)_{p_{c_r}}}{2}, \text{ for } y = 0,1,2,...,N \quad (1)$$

$$k(p^s_i) = z_i,\ i = 1,2,3,...,N \quad (2)$$

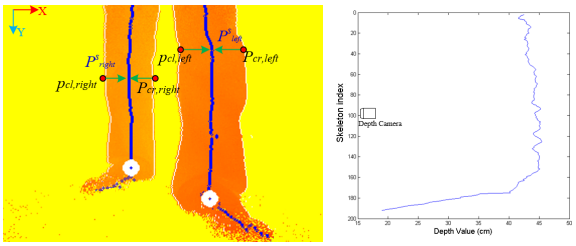

(a) (b)

Figure 3. The construction of skeleton of both leg. (a) The skeletal points were formed by the middle position of the contour along y-axis which display on colormap. (b)The skeleton which depth values of left leg are projected into 2D plane.

The curvature of the skeleton $k''(p^s_i)$ can be derived as equation (3). First, the skeletal points with depth values z are projected onto a 2D curved line, and the second derivative is approximated by second central difference. More specifically, we compute the convolution between $[k(p^s_{i-1})\ k(p^s_i)\ k(p^s_{i+1})]^{\mathrm{T}}$ and second derivative mask [1 -2 1], where $i = 1,2,...,N$. Obviously, the zero curvature indicates a flat line, negative curvature value means the inflection point from convex tuning to concave down, and vice-versa. As shown in Fig. 4(b), we only focus on the least negative curvature of skeleton depth value which is defined as the estimated position of ankle p_{ankle}. Then, we define the estimated top of shank position $p_{\text{top shank}}$ is at top of the skeleton whereas estimated position of tiptoe p_{tiptoe} is placed at the bottom of the skeleton. Finally, the estimated ankle position, top of shank position and tiptoe position can be obtained which is shown in Fig. 4(a).

$$k''(p^s_i) = \begin{bmatrix} k(p^s_{i-1}) & k(p^s_i) & k(p^s_{i+1}) \end{bmatrix}^{\mathrm{T}} \begin{bmatrix} 1 & -2 & 1 \end{bmatrix} \quad (3)$$

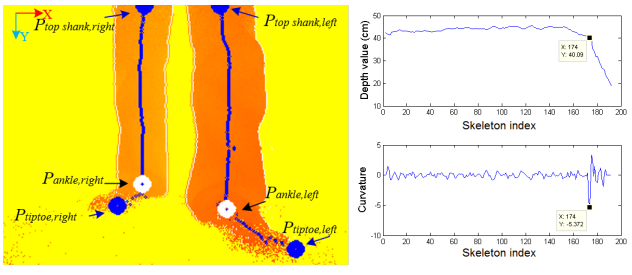

(a) (b)

Figure 4. (a) The estimated position of ankle, top of shank and tiptoe of each leg. (b) The curvature of left leg skeleton, the most curve position as well as the least value of negative curvature indicates ankle position.

B. 3D Leg Pose Tracking

Note that the motion of the human leg is fast and unpredictable. More so, the noise might cause the failure of the leg tracking in the depth image. For instance, the remainder of the outlier point from the RANSAC algorithm are considered

as noise data. In order to deal with the mentioned problems, we formulate the leg pose tracking problem as a Bayesian nonlinear filtering problem. In this section, we adopt the particle filtering approach which uses a finite number of particles to represent the posterior distribution of the target for tracking the leg. Particle filtering approach is an iterative process, and produces a posterior which is the leg pose at each iteration. Moreover, the process halts only when the task of tracking the leg pose is terminated.

1) State Model: Our goal is to estimate the posterior probability $p(\mathbf{X}_t|\mathbf{o}_t)$ at time t. Given observation $\mathbf{o}_t$ mentioned in Section III-B, the configuration of $\mathbf{X}_t$ is a vector of composed of four tapered cylindrical models (different radius of top base and bottom base are different) which represent the estimated models of shank and foot of both legs at time t. The elements in $\mathbf{X}_t$ consists of coordinates of every cylinder base, the widths of cylinders, so that there are a total of 12 elements in $\mathbf{X}_t$.

In the definition of the state model, we consider the natural human leg movement, and various constraints are defined as follows:

1) Intersection between two cylinders are not allowed.
2) When the human user is walking, the positions of shank and foot considered should be reasonable. For example, the position of the shank should be above that of the foot, not the other way around.
3) The maximum and minimum value of width, length, and joint angle (ankle) of each leg model should be constrained with a appropriate value ranges.

The state model in the particle filter process is represented by a set of N weighted particle at time t, which is denoted as follows:

$$\mathbf{s}_t = \{\{s_t^{(1)}, \pi_t^{(1)}\}, \{s_t^{(2)}, \pi_t^{(2)}\}, \cdots, \{s_t^{(N)}, \pi_t^{(N)}\}\} \quad (4)$$

Moreover, the particle set $\mathbf{s}_t$ is used to estimate the optimal model configuration of state X_t by using equation (5).

$$X_t = \sum_i^N s_t^{(i)} \pi_t^{(i)} \quad (5)$$

2) Initialization: In the initialization of particle filter, N particles $\mathbf{s}_t$ are initially sampled for estimating the leg pose at $t = 0$, and the expression can be derived as follows:

$$\mathbf{s}_0 = \{\{s_0^{(1)}, \pi_0^{(1)}\}, \{s_0^{(2)}, \pi_0^{(2)}\}, \cdots, \{s_0^{(N)}, \pi_0^{(N)}\}\} \quad (6)$$

where $\{s_0^{(n)}, \pi_0^{(n)}\}$ is the n-th sampled particle with associated weight π^n.

Each particle represents the predicted leg model(four cylinder models that describe shank and foot of both legs). Instead of a random sampling on the whole image, we place the samples based on the priorly estimated position of p_{ankle}, $p_{\text{top shank}}$, p_{tiptoe} of each leg as mentioned in previous section. The initial sampling of each particle includes the estimated position (ankle, top shank and tiptoe), widths adjust to Gaussian noise with zero mean and manually adjust variance ϵ at $t = 0$. To ensure the shank and foot are connected in predicted leg model of each particle, the center point of bottom base of shank cylinder and the center point of top base of foot cylinder are set as same position which is the estimated ankle position p_{ankle}. As shown in Fig. 5(a), both cylinders (shank cylinder and foot cylinder) use the same position of the p_{ankle} with additive ϵ as position of the bottom base (foot) and position of the top base (shank), respectively. Thus, initial $s_0^{i,3}$ and $s_0^{i,4}$ are the 3rd and 4th element of i-th sampled particle, which are derived as follows:

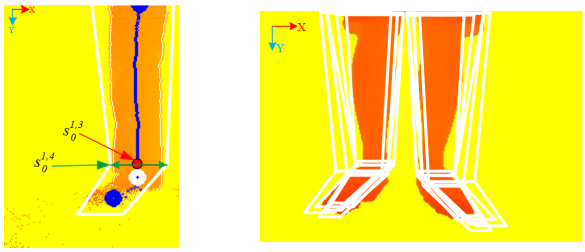

(a) (b)

Figure 5. The initialization of particles display on color map. (a) The 2D cylindrical leg model drawn according to the estimate positions $p_{topshank}$, p_{ankle}, p_{tiptoe} with gaussian noise, where the $s_t^{i,j}$ is the j element of i-th particle at time $t = 0$. (b) The number of particles $N = 5$ were drawn on the color map.

$$s_0^{i,3} = p_{ankle} + \epsilon_{ankle} \quad (7)$$

$$s_0^{i,4} = p_{cr,ankle} - p_{cl,ankle} + \epsilon_{width,ankle} \quad (8)$$

where $s_0^{i,3}$ and $s_0^{i,4}$ are the estimated of ankle joint position and width at the ankle joint adjust to corresponding additive Gaussian noise ϵ. So, the rest of the elements in the particle are similar to the above calculation.

The idea of this modified initialization is to eliminate the particles of irrelevant samples such that when the shank cylinder and foot cylinder are not connected within a particle sample, and to prevent the initial particles which are sampled too far away from the foreground in the depth image. As shown in Fig. 5(b), the particles are drawn according to the estimated position of p_{ankle}, $p_{\text{top shank}}$, p_{tiptoe} with addictive ϵ. In the meanwhile, the sampling of particles must obey the constraints which are defined in state model.

3) Motion model: Motion model is the state transition model that characterizes the motion change over time. According to [7], [8], it is claimed that the human leg is conducting a simple harmonic motion (SHM) during walking, and the human gaits can be considered as a sequence motion of the leg separated into two motion phases namely, stance phase and swing phase. The equation (9) and (10) illustrate how we apply the SHM into motion model in the particle filter:

$$x_{t+1} = x_t + \epsilon \quad (9)$$

$$y_{t+1} = y_t + Acos(\alpha t - \varphi) + \epsilon \quad (10)$$

The point elements of sampled shank and foot cylinders at time $t+1$ are represented by x_{t+1} and y_{t+1} in depth image, respectively. In equation (10), A is the amplitude of SHM

and also the swing range of leg, α is the angular velocity of leg, φ is phase difference of SHM, t represents the time sequence, and ϵ is Gaussian noise with it's variance σ.

We see that SHM only happens mostly in the vertical direction (y direction in depth image) at each time slice, because human moves mainly forward let the horizontal direction motion can be just approximated by a Gaussian noise as shown by equation (9). For obtaining the above parameters in SHM, we preset some fixed parameters as initialization, such as that the positions of the ankle p_{ankle} and p_{tiptoe} are recorded for estimating the amplitude and period as the new arguments for the motion model in particle filter. Of course, we keep updating the parameters to make sure our motion model will fit the real motion of leg as much as possible.

4) Computation of The Particles Weights: The weight π of the particles at time t can be computed by weighting function $w(\mathbf{X}_t|\mathbf{o}_t)$ given by the observation $\mathbf{o}_t$, where $w(\mathbf{X}_t|\mathbf{o}_t) \propto \pi_t$. Before we calculate the weighting function, the two image features are introduced. First, we propose the edges map of the lower limb, which provides the useful information like contour of lower limb in depth image. Canny edge is used to produce the edges map, and we adjust the threshold to remove the spurious edges, as shown in Fig. 6(a).

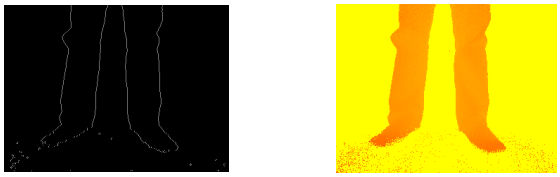

(a) (b)

Figure 6. (a) Edge map. (b) Foreground depth image displays on color map.

The mean square error function is derived as follows:

$$E_{contour}(\mathbf{X}, o_e) = \frac{1}{N}\sum_{i=1}^{N}(1 - d_i^e(\mathbf{X}, o_e))^2 \qquad (11)$$

where o_e is edges map of observation and $\mathbf{X}$ is the vector of the sampled cylindrical model, and $d_i^e(\mathbf{X}, o_e)$ is the pixel in edges map locates along the cylinder model's contour as can be seen in Fig. 7(a).

Fig. 6(b) shows the second feature, namely, foreground of depth image, which is fully described in Section III. Mean square error function is computed with particle and a set of foreground points o_f:

$$E_{interior}(\mathbf{X}, o_f) = \frac{1}{N}\sum_{i=1}^{N}(1 - d_i^f(\mathbf{X}, o_f))^2 \qquad (12)$$

where $\mathbf{X}$ is the vector of the sampled cylindrical model and $d_i^f(\mathbf{X}, o_f)$ is the foreground point belonging to the interior of the sampled cylinder of i-th particle, which can be found in Fig. 7(b).

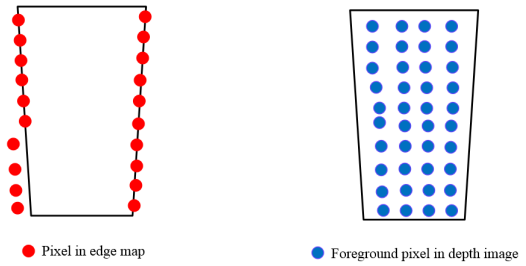

(a) (b)

Figure 7. The proposed two features for weighting a particle. (a) Measurement based on sampling on edges map, d_i^e computes the pixels (red dots) locate along the contour of cylinder's surface, in this case the $E_{contour}(\mathbf{X}, o_e) = 0.2$; (b) Measurement based on sampling on the foreground points, d_i^f computes the pixels (blue dots) belong to the interior of cylinder's surface, in this case the $E_{interior}(\mathbf{X}, o_f) = 0$.

Then, we assign the weight of particles by adding two mean square error function of $E_{contour}$ and $E_{interior}$ together, and the exponentiated result to give:

$$w(\mathbf{X}, \mathbf{o}) = \exp -(E_{contour}(\mathbf{X}, o_e) + E_{interior}(\mathbf{X}, o_f)) \qquad (13)$$

In equation (14), we can easily get the idea that the value of weight is inversely proportional to the errors in the sense that the value of weight is greater as the summation of errors is smaller.

Finally, given the observation $\mathbf{o}_t$, the posterior probability $p(\mathbf{X_t}|\mathbf{o}_t)$ of tracking result can be computed with the summation of weights among N particles at time t:

$$p(\mathbf{X}_t|\mathbf{o}_t) = \frac{1}{N}\sum_{i}^{N} w_t^i(\mathbf{X}_t, \mathbf{o}_t), \text{where } i = 1, 2, ..., N \qquad (14)$$

IV. Gait Analysis

As shown in Fig. 8, human walking gait is a periodic movement of each limb from one position of support to next position. The single sequence of the functions by one limb is called gait cycle. The gait cycle basically has two components, swing phase and stance phase. Stance phase means the foot is in contact with the ground. Swing phase means the foot is swinging in the air for creating a new step forward. In the scenario of walker user, the user walks toward the depth camera, swing and stance phase can be easily determine as the system has tracked the foot position p_{ankle} and p_{tiptoe}. More specifically, the swing and stance phase can be distinguished by calculating the distance between foot (ankle position p_{ankle}, tiptoe position p_{tiptoe}) and floor. The distance between position of foot and floor approaches to zero when the foot in stance phase, and the swing phase occurs when foot position is far away from floor. Through the benefit of the pattern of gait cycle, the spatio-temporal gait parameters can be easily determined.

Since the tracked leg pose is obtained by particle filter in Section III-B, spatio-temporal gait parameters can be calculated. Here, we focus on monitoring step length and step

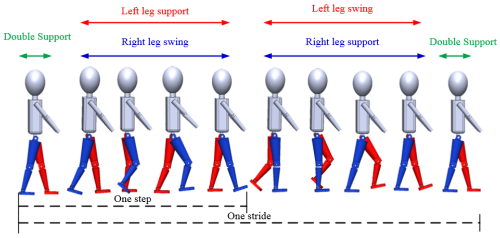

Figure 8. Typical human walking cycle.

velocity of user in our system. The stride length $L_{stride}(i)$ is the distance between support phase and the next support phase of same foot which is between i to $i+1$-th step, and step length $L_{step}(i)$ is defined as the distance between the both feet in i-th step. Step velocity $V_{step}(i)$ means the speed from $i-1$ step length to i-th step length.

As Fig. 9 shows recorded experimental data of the y-axis (vertical axis) of foot position with respect to the depth camera, which indicates the height between the foot position and ground. In terms of the gait phase, the height of foot increase when the foot is lifting up which in swing phase, whereas the height tiptoe is approximately equal to zero in which the foot supports on the ground.

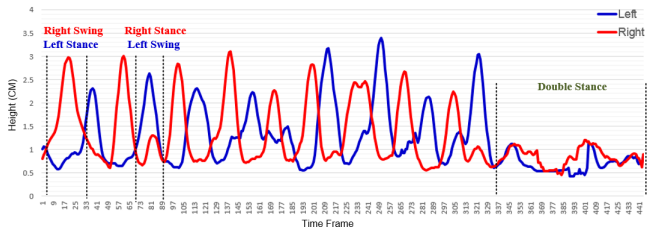

Figure 9. The recorded trajectory of y-axis of foot position with respect to depth camera. The height between foot and ground are marked as stance phase and swing phase.

Due to the scenario of the user's walking assisted by the walker, the continuous variation of distance between foot and depth camera (Fig. 10) provides us the motion of walking gait. Note that the speed of the walker is the speed of the user. When the moment of distance between foot and camera become closer which means the foot is performing swing phase as well as approaching to the camera until the foot contacted with ground. On the contrary, the stance phase happen when distance between depth camera and foot getting farther away from the camera, the increasing of the distance in behalf of the robotic walker is moving forward and cause the camera far from the support foot. Once the foot is determined that touched the ground, the step length (length between both leg) and stride length (displacement of single leg) can be calculated.

V. Experiment

In this Section, the system evaluation will be presented. The comparison of accuracy rate between our system and motion capture system will be introduced. We calculate the

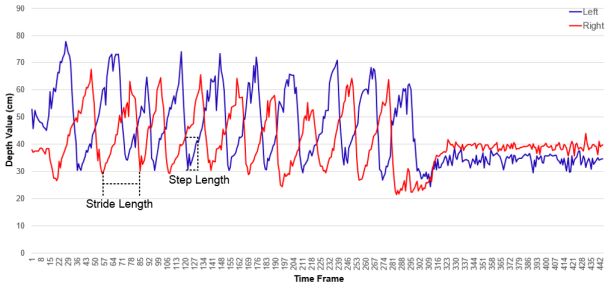

Figure 10. The real recorded data from experiment which indicates depth value of foot.

error rate of stride length compare with the result of motion capture system. In addition, the gait phase is verified by the human labeled ground truth.

Spatio-temporal gait parameters such as step length is important determinant of fall risk and gait variability. Thus, result of the proposed 3D tracking and gait analysis need to have inspection and verification on spatio-temporal gait parameters. To validate the proposed gait analysis system, the commercial 3D motion capture system, Phase Space [9] was used as ground truth to validate our system.

In the experiment, we collected walking gait data of one subject who used the walker and walked forward with normal gait for 5 meters in aforementioned experiment environment. In another aspect, the walker moved forward according to the subject mean velocity for capturing the subject's steps. There are totally five trials in the experiment and we recorded both of the 3D points of $p_{topshank}$, p_{ankle} and p_{tiptoe} from proposed method and 3D position of marker from motion capture system for the entire process. In the system specification, the system software was implemented in C++ and the current running time was average 25 FPS with 100 particles including the depth image processing.

The error rate of step length are shown in Table I. Obviously, the proposed 3D leg tracking with particle filter had smaller error rate than non-using one. The poor result of non-using particle filter impute to the noise arise from the outlier of floor segmentation, noise from the floor may lead the detection error of the foot position whereas the proposed 3D leg pose tracking with particle filter can deal with influence of noise or missing data in depth image. Fig. 11 shows the result of the proposed 3D leg pose tracking using particle filter, the missing data occurred at frame 180 to 220 around the position of tiptoe of left leg in the depth image, but the tiptoe position p_{tiptoe} still being tracked successfully. Moreover, Fig. 12(a) (tracking without particle filter) shows the tracking result is influenced by the noise of outlier of floor segmentation and which is the main reason for error, and the tracking with particle filter (Fig. 12(b)) can successful track the leg pose.

For the verification of the gait phase, we compare our result with human labeled data to find the performance. Referring to Table II,there are totally 1654 images were recorded from the each trial of the experiment, and those images were manually classified into four categories, which

TABLE I. The mean and standard deviation of step length error of the proposed 3D leg tracking with particle filter and non-using particle filter.

Trial	W/o Particle Filter		With Particle Filter	
	Mean (cm)	**STD (cm)**	**Mean (cm)**	**STD (cm)**
1	7.05	6.51	2.84	2.11
2	6.61	7.02	1.96	0.71
3	4.38	2.77	1.71	1.66
4	5.3	4.68	2.16	0.87
5	6.38	3.61	2.95	1.25
Mean	6.03		2.33	

TABLE II. The correct rate of gait phase against to ground truth.

Trial	**Frames**	**Correct Rate (Percent)**
1	342	88.6
2	250	91.1
3	370	82.8
4	302	86.7
5	390	83.2
Mean		86.5

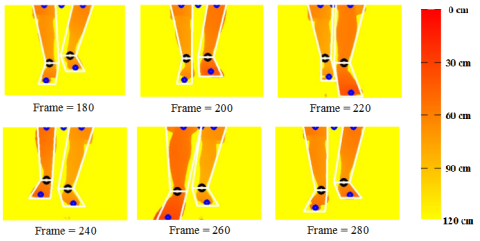

Figure 11. A demonstration of proposed 3D leg tracking using particle filter.

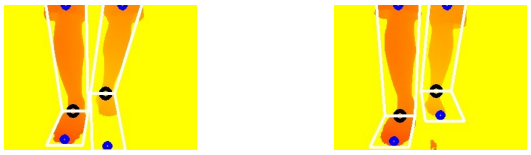

(a) (b)

Figure 12. (a) The 3D leg pose tracking without particle filter. (b) The 3D leg pose tracking with particle filter.

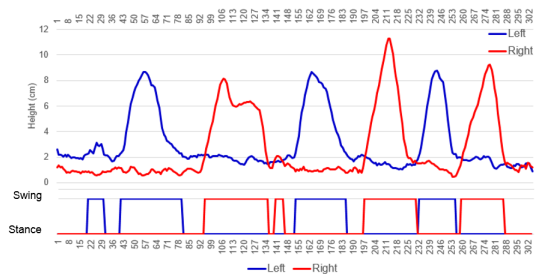

Figure 13. The outcome of the gait phase based on the height of foot position.

are left leg stance,right leg stance, left leg swing and right leg swing. The overall correct rate is 86.5 percent against to the ground truth. As Fig. 13 shows the majority of errors emerge at the moment of transition of gait phase as a result of the missing data. Most of the errors are usually arise in a short period; thus, it is difficult to perceive by human when the errors occurred.

VI. Conclusion

In this work, we propose a completely non-intrusive gait analysis method on an active robotic walker, where the spatio-temporal gait data can be obtained by tracking lower limb movement in real time.

First of all, the system removes redundant information to extract the part of lower limb such as background and floor. Next, leg segmentation is conducted before the leg pose is being tracked. Then a reliable 3D leg pose tracking is proposed by using particle filter, the real time tracking is accomplished by the modified particle sampling process with identifying the feature of ankle in depth image. Finally, the gait parameters such as step length and step velocity can be extracted in gait analysis.

In the experiment, the accuracy rate of 3D leg pose tracking and gait analysis is validated by comparing with commercial motion capture system. The average error rate of the step length by the proposed tracking method is 2.33 cm. The experiment results show that our system can track human leg pose successfully and verify gait phase correctly.

Acknowledgements

This research is supported by Ministry of Science and Technology of the Republic of China in Taiwan under granting from NSC 102-2218-E-002-009-MY2. Thanks for Taoyuan Veterans Home, VAC in Taiwan and all the patients and staff who participate in these experiments.

References

[1] J. Saboune, C. Rose, and F. Charpillet, "Factored interval particle filtering for gait analysis," in *29th Annual International Conference of the IEEE Engineering in Medicine and Biology Society,* pp. 3232–3235, 2007.

[2] M. Goffredo, I. Bouchrika, J. N. Carter, and M. S. Nixon, "Self-calibrating view-invariant gait biometrics," *IEEE Transactions on Systems, Man, and Cybernetics,* vol. 40, no. 4, pp. 997–1008, 2010.

[3] M. Goffredo, J. N. Carter, and M. S. Nixon, "Front-view gait recognition," in *2nd IEEE International Conference on Biometrics: Theory, Applications and Systems,* pp. 1–6, 2008.

[4] E. Auvinet, F. Multon, and J. Meunier, "Lower limb movement asymmetry measurement with a depth camera," in *Annual International Conference of the IEEE Engineering in Medicine and Biology Society,* pp. 6793–6796, 2012.

[5] R.-L. Hu, A. Hartfiel, J. Tung, A. Fakih, J. Hoey, and P. Poupart, "3d pose tracking of walker users' lower limb with a structured-light camera on a moving platform," in *IEEE Computer Society Conference on Computer Vision and Pattern Recognition Workshops,* pp. 29–36, 2011.

[6] M. A. Fischler and R. C. Bolles, "Random sample consensus: a paradigm for model fitting with applications to image analysis and automated cartography," *Communications of the ACM,* vol. 24, no. 6, pp. 381–395, 1981.

[7] D. Cunado, M. S. Nixon, and J. N. Carter, "Automatic extraction and description of human gait models for recognition purposes," *Computer Vision and Image Understanding,* vol. 90, no. 1, pp. 1–41, 2003.

[8] L. Xuejun, Z. Meng, and Z. Lingxia, "The study for dynamic model of gait," in *IEEE 14th International Conference on Computational Science and Engineering,* pp. 551–554, 2011.

[9] PhaseSpace Inc. Phasespace 3d motion capture system. [Online]. Available: http://www.phasespace.com/